World Journal of Advanced Research and Reviews
eISSN: 2581-9615 CODEN (USA): WJARAI
Cross Ref DOI: 10.30574/wjarr
Journal homepage: https://wjarr.com/

(RESEARCH ARTICLE)

Check for updates

Coulomb Stress Analysis And Monte Carlo Simulation In Predicting Sinabung Pyroclastic Flow

Goldberd Harmuda Duva Sinaga [1,*], Switamy Angnitha Purba [2] and Ady Frenly Simanullang [3]

[1] *Mechanical Engineering, Universitas HKBP Nommensen Pematangsiantar, North Sumatra, Indonesia.*
[2] *Mathematics, Universitas HKBP Nommensen Pematangsiantar, Pematangsiantar, North Sumatra, Indonesia.*
[3] *Physics Education, Universitas HKBP Nommensen Pematangsiantar, Pematangsiantar, North Sumatra, Indonesia.*

World Journal of Advanced Research and Reviews, 2022, 13(01), 781–792

Publication history: Received on 20 December 2021; revised on 29 January 2022; accepted on 30 January 2022

Article DOI: https://doi.org/10.30574/wjarr.2022.13.1.0085

Abstract

Sinabung is a small stratovolcano located in northern Sumatra about 50 km northwest of the Toba caldera. On August 27, 2010, it was confirmed that Sinabung experienced a phreatic eruption for the first time in history. Initially the eruption formed a lava dome that fell out on January 10, 2014 forming pyroclastic density currents. An increase in pore fluid pressure in the crust supports Coulomb Failure Friction. Positive coulomb stress values are thought to trigger Sinabung activity. The research uses a combination of Monte Carlo simulation to predict the next earthquake parameters and coulomb stress analysis to determine the direction and value of stress . The Monte Carlo simulation produces earthquake parameter prediction, longitude 98^{o} latitude 3.175^{o} depth 104.5 meters, Mw 6.0, strike 28.125 ^{o}, slip 42^{o}, dip 44.17^{o}. Coulomb Stress analysis of the combined 2001-2021 earthquake data produces an average coulomb value of 0.24 bar, 0.14 bar shear, 0.25 bar normal and the direction of the stress vector to the southwest of Mount Sinabung. The results of the combined coulomb stress analysis and Monte Carlo simulation predict the direction of pyroclastic flows to the northeast, east, and southeast of Mount Sinabung, in accordance with the direction that is inversely proportional to positive stress so that the area needs to receive early warning of volcanic eruption natural disasters in 2022.

Keywords: Coulomb Stress; Monte Carlo; Pyroclastic; Sinabung

1. Introduction

Sinabung is a small stratovolcano with a diameter of <5 km and an altitude of 2460 m (1,000 m above the surrounding countryside). It is located in northern Sumatra about 50 km northwest of Toba caldera. This is motivated by the Toba Caldera, which was produced by the eruption of the VEI 8 index at 74,000 years ago. Prior to 2010, Sinabung was classified by the Center for Volcanology and Geological Hazard Mitigation (PVMBG) as a "B-type" volcano, which has not erupted in modern history since 1600 AD (1) .The first sign of increased Sinabung activity in the peak area, was detected with interferometric synthetic aperture radar during the period 2007-2010 (2)(3). Sinabung experienced a phreatic eruption—the first confirmed eruption in a historic time (1)(4)(5). Sulfur dioxide emissions were detected by the Aura/Ozon Mapping Instrument on August 27, 2010. In retrospect, this 2010 eruption was the opening stage of what has been a prolonged eruption with major impacts on the community and economy of the area (6). The ongoing effusive phase of the eruption of Mount Sinabung (Sumatra, Indonesia) began in late December 2013, and has produced a 2.9 km long andesite lava flow with two active secondary peak lobes, and frequent pyroclastic density currents (PDC) (≤ 5 km runout distance) with related feathers up to > 5 km high. The lava that erupted first formed a lava dome (the first dome growth and collapse phase) (7) which completely collapsed on January 10, 2014 forming pyroclastic density currents (PDCs).

* Corresponding author: Goldberd Harmuda Duva Sinaga
Mechanical Engineering, Universitas HKBP Nommensen Pematangsiantar, North Sumatra, Indonesia.

The importance of changes in pore fluid pressure for earthquake generation has been well known (8)(9)(10)(11)(12). The increase in pore fluid pressure in the crust reduces the normal stress on the fault, which supports coulomb failure friction. Pore fluid pressure also affects the mode of magma transport by playing a role in the failure of magma reservoirs. In theory, an increase in pore fluid pressure can trigger an eruption without an increase in reservoir pressure, which may be the explanation for why some eruptions occur without significant inflation before an eruption. The position of the mountain against the fault, active tectonic conditions, changes in coulomb stress, as well as the tendency towards rupture can explain the extent of the causal relationship. There are two approaches to coulomb stress changes, the first by considering geometry and rake on faults, and the second by being concentrated on tectonics and regional stress. Positive coulomb stress value is suspected to trigger liveliness in the area caused by previous large earthquakes. Coulomb stress change before the eruption of Mount Sinabung caused by both the 2004 Aceh earthquake and earthquakes with magnitudes above 7 SR resulted in some areas experiencing stastic deformation. From seismicity plots, most earthquakes occur in areas with positive coulomb stress changes. Positive coulomb stress also occurred in the area of mount Sinabung which triggered a disturbance in the sinabung magma kitchen that fell asleep for 400 years. The eruption was preceded by 4 shallow tectonic earthquake events caused by the activity of the Sumatra Great Fault around Mount Sinabung and 2 tectonic earthquake events with shallow-medium depth caused by subduction zones. The location of the earthquake is relatively close to Mount Sinabung with Mw>6.0. The approval of the sloping megathrust subduction makes sinabung magma chambers at shallow-medium depths emit phreatic eruptions. This is indicated by the presence of two shallow-medium depth earthquake events (13). Monte Carlo is a computational algorithm to simulate various behavioral physical and mathematical systems. This method proved efficient in solving differential equations, radians field integrals. Monte Carlo methods are generally performed using computers and using computer simulation techniques (14). The Monte Carlo method is a method of numerical analysis that involves sampling randomized number experiments. A positive function f(x) as shown in the formula below with the distribution of points scattered all the same (uniform), where the part of the points below the function curve (x) is close to the ratio of the area below the curve of the rectangular area.

2. Material and methods

The method used is a combination of descriptive analytical, namely with explanation through a combination of coulomb stress model and Monte Carlo Simulation. The models used in the study were the coulomb stress and Monte Carlo models. The data needed in analysis and simulation is earthquake data in the form of earthquake location, magnitude, depth, earthquake type, strike, slip, dip, and tensor moment. Earthquake data 2001-2021 analyzed in Coulomb software 3.3 then produce changes in Coulomb Stress in bar units in positive or negative form then the earthquake data is analyzed in Monte Carlo simulations to predict the value of subsequent earthquake data. The simulation results were reanalyzed in Coulomb 3.3 so as to obtain vector direction and positive stress distribution values in the form of 2D (15) and 3D maps of mount Sinabung pyroclastic flows. With this combination of methods, tectonic earthquake distribution data can predict the pyroclastic flow of Mount Sinabung.

2.1. Analysis of Coulomb Stress

Failure of faults is thought to be caused by a combination of normal (reduced) and shear stress conditions, generally measured as static coulomb stress criteria (16). Static coulomb stress caused by earthquakes may help explain the distribution of aftershocks.(17) since aftershocks will occur when Coulomb stress exceeds the collapse strength of the fault surface. Coulomb Stress status (ΔCFF) is defined as

$$\Delta CFF = \Delta_\tau + \mu\,(\Delta_\sigma + \Delta p)$$

Δτ represents the change in the shear stress on the fault (positive in the direction of the slip), Δσ is the change in normal stress (positive for unclamping fracture), Δp is the change in pore pressure, and μ is the coefficient of friction, which ranges from 0.6 to 0.8 for most intact rocks (18). In this area of Oklahoma, where fluid injection is 1-2 km deep near the epicenter, Having been used for disposal since 1993 (19), the influence of pore pressure cannot be ignored. Changes in pore pressure after stress change, in which there is no fluid flow (undrained condition), is

$$\Delta p = \frac{\beta \Delta \sigma_{kk}}{3}$$

where β is the Skempton coefficient and σkk is the number of diagonal elements of the stress tensor (20). The Skempton coefficient describes changes in pore pressure resulting from externally applied stress changes and often their values range from 0.5 to 1.0 (21)(22)(23). For fault zone rhology, where fault zone material is more resilient than surrounding material, $\sigma_{xx}=\sigma_{yy}=\sigma_{zz}$ (24)(17)(17)(18); so, $\frac{\Delta\sigma_{kk}}{3} = \Delta_\sigma$. Equations (1) and (2) combined with this assumption

$$\Delta CFF = \Delta_\tau + \mu \Delta_\sigma$$

Where $\mu' = \mu (1-\beta)$ is the effective coefficient of friction. The effective coefficient of friction generally ranges from 0.0 to 0.8, but is usually found to be around 0.4 ($\mu = 0.75$, $\beta = 0.47$) for horizontal faults or faults whose orientation is unknown (25). These values are commonly used in calculations of coulomb stress changes to minimize uncertainty (26)(27)(28).

The location and geometry of the fault source, as well as the distribution of slips over the source plane, play an important role in calculating changes in coulomb stress. Based on earthquake magnitude, we modeled the source of geometry with empirical relationships (29) for strike-slip faults, which were built into Coulomb 3.3 software (15).

2.2. Monte Carlo Simulation

One of the most popular simulation models on inventory control is the Monte Carlo simulation. Monte Carlo simulation model is a form of probabilistic simulation in which the solution of a problem is given based on the process of randomization (random). This random process involves a probability distribution of data variables collected based on past data as well as theoretical probability distributions. Random numbers are used to describe the random events at all times of random variables and sequentially follow the changes that occur in the simulation process (30).

Imperical Data distribution, namely: the function of Frequency Distribution Probobility,

$$\frac{n}{N} = \int_w^s f(x)dx/[i(w-s)]$$

Where:

N = the number of points (area) in the rectangle created by the f(x) curve

n = number of dots (area) below the curve f(x)

s = lower limit of function f(x)

w = upper limit of function f(x)

i = maximum value of function f(x)

- The distribution of such requests is changed in the form of functions. Commulative Frequency Distribution,
- Each such request, given a limit pointer number (Tag/Label number), is organized on the basis of the Commulative Distribution frequency of the demand distribution.
- Make random number withdrawals, with one form of Random Number Generation (RNG), namely by using the Linear Congruent Method method

(LCM) Xi+1=(a.X1+c) Mod M

With conditions a, c < M , X 0 > 0

3. Results and discussion

3.1. Coulomb Stress Analysis of Pyroclastic Flow

Geologically, Mount Sinabung, is a (13), is one of the stratovolcano type volcanoes in Indonesia. Mount Sinabung is located in Naman Teran District, Tigan Derket Subdistrict, Umbrella Subdistrict, Simpang Empat Subdistrict, and Merdeka District in Karo Regency, North Sumatra Province and geographically Mount Sinabung is at latitude 3° 10' and longitude 98° 23.5' with an altitude of 2,460 meters above sea level. (31)

Based on earthquake data obtained from the Global CMT website for 20 years starting from 2001 to 2021, the number of 995 events obtained with a limit value of 5.0-9.00 Mw. But researchers re-limit coulomb stress data analysis starting from 9.0 to 5.5 Mw. This is done because coulomb software 3.3 has a limit of 127 data inputs.

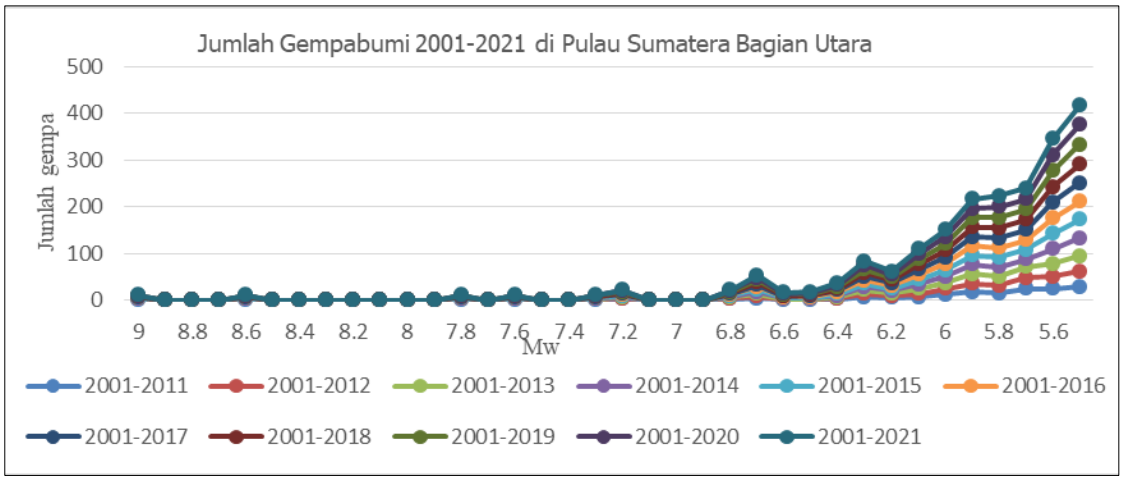

Figure 1 Number of earthquakes 5.6-9.0 Mw in 2001-2021 in northern Sumatra

Based on figure 1 since the 9.0 Mw earthquake that occurred in Aceh in 2004, the Indian Ocean and Sumatra island area experienced an increase in tectonic activity until now. The number of earthquake increases from 2001-2011 to 2001-2021 has an average increase of 21 times each year, with the highest number of increases occurring in 2012 and the lowest occurring in 2021. Figure 1 describes that earthquakes that often occur are earthquakes that have a magnitude of 5.6 Mw while the most rare is earthquakes with a magnitude of 9.0 Mw. Earthquake data displayed in the table is the earthquake data that will be analyzed in Coulomb 3.3 software. The data is then analyzed so that shear, normal, and Coulomb values are obtained and the direction of distribution of stress / strain from earthquakes that occur.

Earthquake data analyzed in Coulomb 3.3 software produced average shear, normal, and Coulomb values that vary from year to year. The highest Coulomb average value occurred in 2015 at 0.23 bar while the smallest Coulomb average was 0.1079 bar.

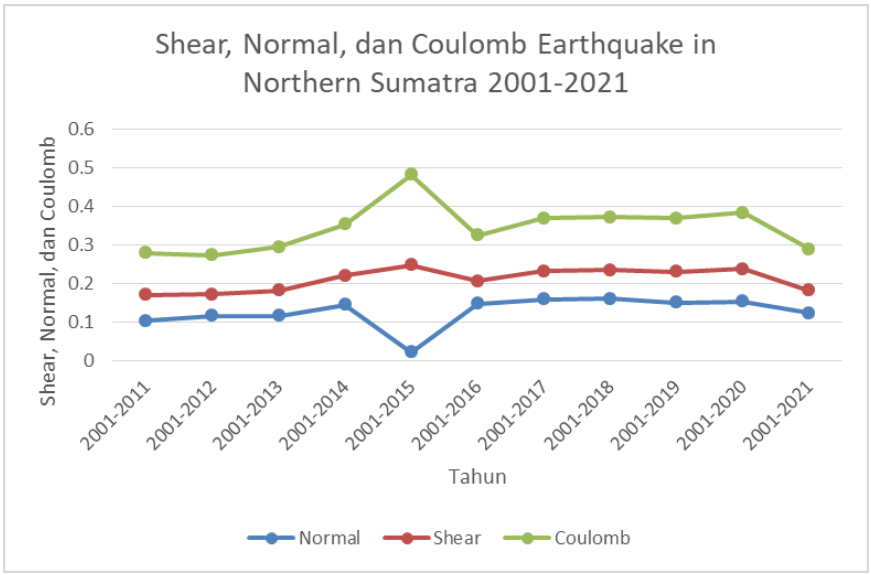

Figure 2 Shear Values, Normal, and Changes in Coulomb Stress Earthquake in northern Sumatra

Likewise, the highest average shear value occurred in 2015 at 0.226 bar while the lowest shear value also occurred in 2021 at 0.058 bar. But the highest normal value actually occurred in 2018 at 0.16 bar while the lowest normal value occurred in 2015 at 0.021 bar. Based on the data and also the concept of coulomb stress it is known that the value of shear and coulomb is inversely proportional to the normal value.

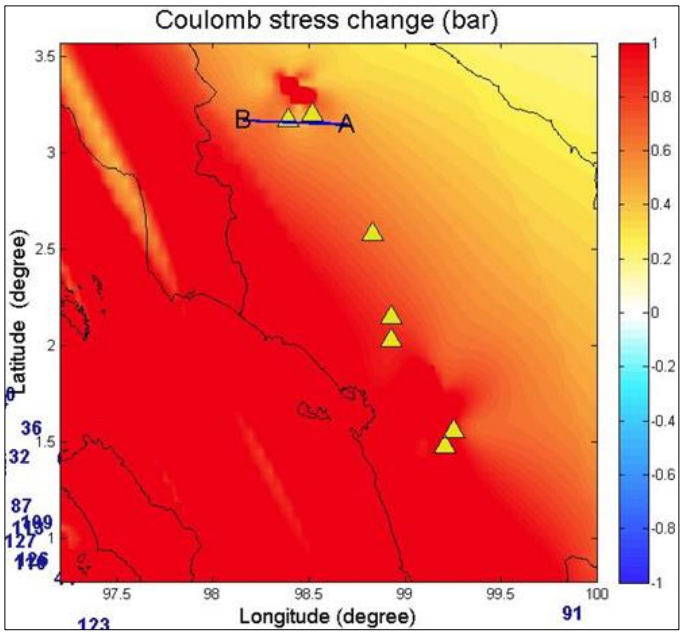

Figure 3 Spread of Coulomb Stress Change on Mount Sinabung

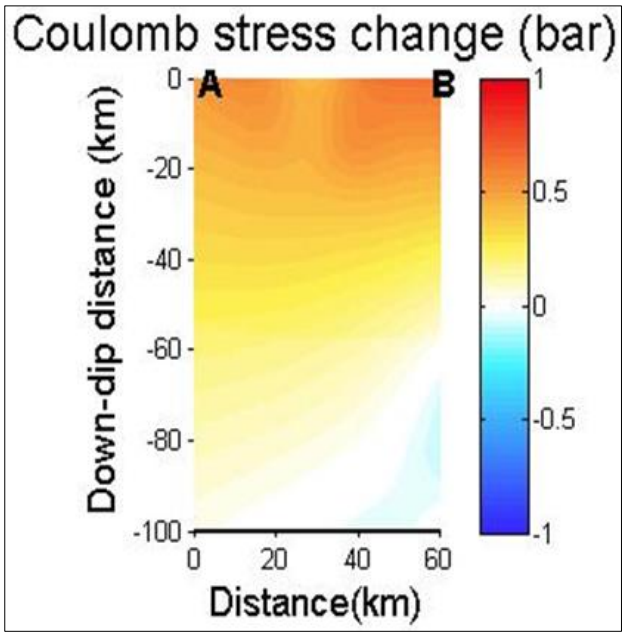

Figure 4 Spread of Coulomb Stress Change on Mount Sinabung in depth of 0-100 km

Figure 3 is one of the case studies of Mount Sinabung which experienced a spread of positive coulomb stress changes in 2021 marked by red lobes while figure 4 is the result of cross section obtained from the distribution of coulomb stress changes under Mount Sinabung in 2021 at a depth of 0-10 km. In the image of cross section A-B in areas that experience increased stress is more inclined to the north and partly to the west-southwest. Cross section results have a shear value of 0.05, a normal 0.12 bar, and a Coulomb of 0.1 bar.

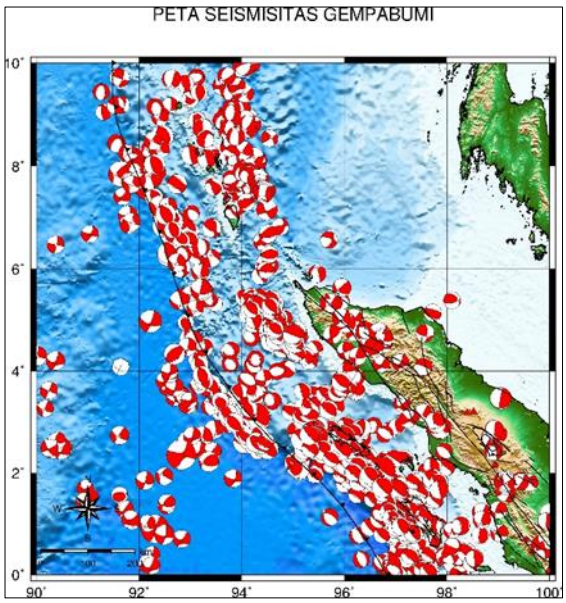

Figure 5 Earthquake distribution map with Centroid Moment Tensor in 2021

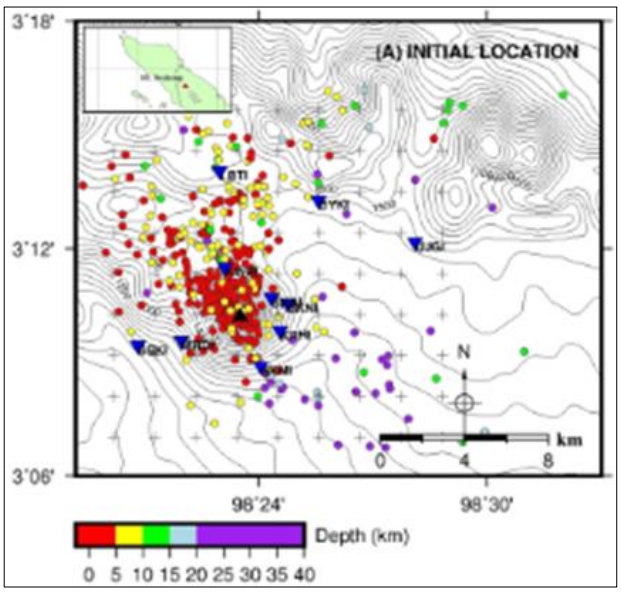

Figure 6 Map of hypocenter distribution of VT earthquake on Mount Sinabung (initial location)

Figure 5 shows a map of the distribution of earthquakes with centroid tensor moments from each event that occurred in 2021. Centroid moment tensor that shows strike-slip fault, reverse fault, and normal fault. The distribution of earthquakes is influenced by regional geological conditions.

Increased changes in coulomb stress affect seismic around Mount Sinabung. The effect of increased coulomb stress changes occurs in the increasing number of hypocenter points of VT earthquakes according to 3D seismic tomography research from Mount Sinabung (31). One of the effects can be seen from the increase in coulomb stress changes in 2010 to 2013 which increased every year. The increase in the number of hypocenter VT earthquakes from 2010 to 2013 can be seen in figure 6 and figure 8.

Likewise with the number of hypocenter VT earthquakes located within the depth. The number of hypocenter VT earthquakes (after relocation) located at a depth of more than the hypocenter VT earthquake (initial relocation). A comparison of this number can be seen in figure 7 and figure 9. Figure 6 and figure 8 show most earthquakes located under buildings with depths between -2.4 and 6 km below sea level on average (meters above sea level). The deepest VTs are below the summit and extend to depths of 38 km.

The seismicity of distal VT is concentrated in the northwest, north, northeast and southeast. Network configurations block locations in sectors that extend from the counterclockwise west to the southeast (31). Overall, VTs are the displacement of seismic network boundaries that are centralized to the north and peak to the northwest with shallower depths (maximum depth of 38 km) on Figure 6. (31)

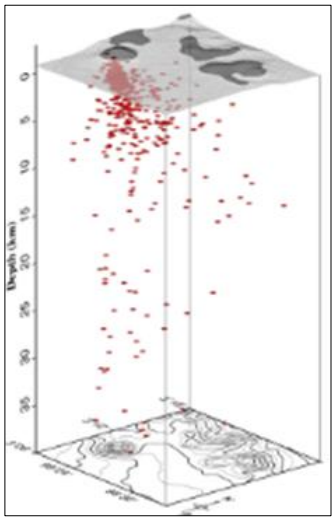

Figure 7 Map of the hypocenter distribution VT earthquake on Mount Sinabung (initial location) at a depth of 0-40 km

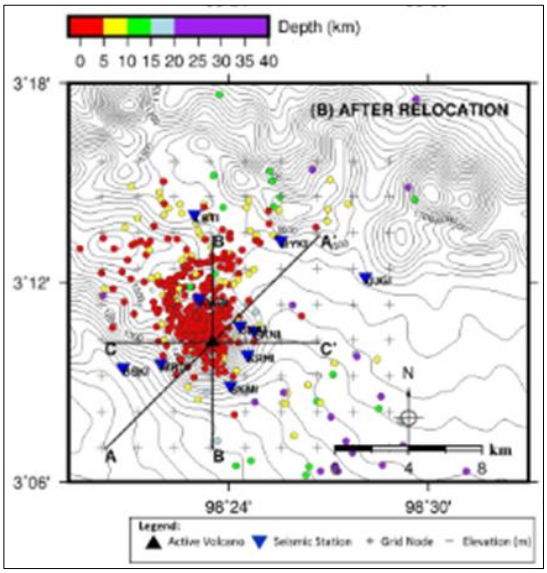

Figure 8 Map of hypocenter distribution VT earthquake on Mount Sinabung (after relocation) at a depth of 0-40 km

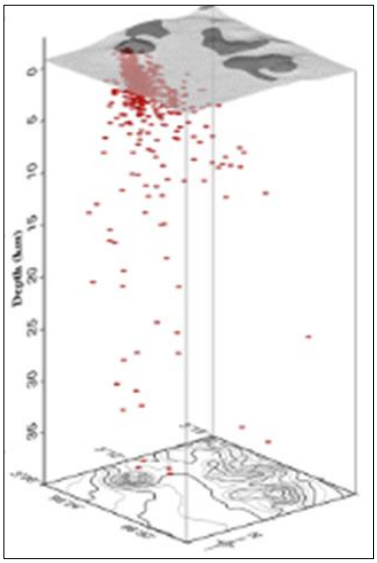

Figure 9 Map of hypocenter distribution of VT earthquake on Mount Sinabung (after relocation) at a depth of 0-40 km

This phenomenon is appropriate and supports previous research stating that the increase in volcanic activity of Mount Sinabung is due to the situation in the Sinabung region which experiences a large compressive force (13). Similar cases also occurred in Pidie Jaya (32), Palu-Donggala (33), Bengkulu (34), Mount Soputan, Mount Gamalama and several mountain ranges in Indonesia, whose increased activity was affected by increased changes in coulomb stress characterized by red lobes (35)(36)(37). Some areas outside Indonesia are under Coulomb Stress research such as Turkey, Nepal, Iran, Japan, and in countries that are in the path of the ring of fire (38)(39)(40).

3.2. Monte Carlo Simulation Results

Monte Carlo simulation has a stochastic nature which means that this method is based on the use of random numbers and the possibility to identify a problem, this method was previously used to solve quantitative problems with physical processes. In terms of settlement with the Monte Carlo method that will be done is to determine the occurrence of

earthquakes 20 years in a row on the island of Sumatra and the Indian Ocean, namely longitude, latitude, depth, fault type (strike, dip, slip), and Mw (magnitude moment).

Table 1 Monte Carlo Simulation Results from *Strike, Dip, Slip*, Mw, *Longitude, Latitude*, and depth

No	Strike	Fr	Dip	Fr	Slip	Fr	Mw	Fr	Long	Fr	Lat	Fr	*depth*	Fr
1	0-45	4	0-15	35	0-45	1	5.1-6	79	92-94	29	-9-1	30	0-45	104
2	46-90	6	16-30	54	46-90	45	6.1-7	41	95-97	75	2-4	47	46-90	20
3	91-135	12	31-45	14	91-135	48	7.1-8	5	98-100	23	5-7	18	91-135	2
4	136-180	9	46-60	7	136-180	33	8.1-9	2			8-10	32	136-180	0
5	181-225	1	61-75	6									181-225	1
6	226-270	1	76-90	11										
7	271-315	47												
8	316-360	47												
Simulation result		28.125		44.17		42		6		98		3.175		104.5

Tables 1 are Monte Carlo simulations of earthquake data (magnitude moment, strike, dip, slip, longitude, latitude, and depth) in the Indian Ocean and northern Sumatra island from 2001-2021. Monte Carlo simulation results are the result of calculation of distribution tables, probability and cumulative distribution, random numbers, and simulation of random trial series. Tables 1 are also the result of Monte Carlo simulation calculations resulting in predictions of earthquake data that may occur in 2022. The prediction data is also the result of a Monte Carlo simulation which is then analyzed again in Coulomb 3.3 software so that the direction and value of coulomb stress changes positive /negative from Mount Sinabung.

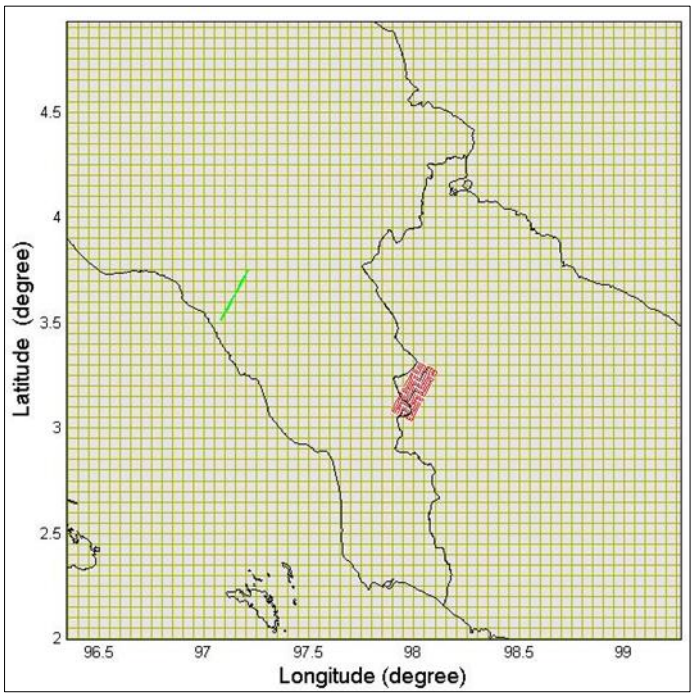

Figure 6 Geometric Map of Fault Sources which is the result of Monte Carlo Simulation

Figure 6 shows a geometric map of the source of the fault which is the result of a Monte Carlo simulation. The geometry of the earthquake is located at a longitude of 98°, latitude of 3,175°, depth of 104.5 km, magnitude moment 6, strike 28.125°, dip 44.17°, rake 42°. If the earthquake in figure 6 is analyzed in Coulomb 3.3, then the positive stress coulomb

leads to the northeast and southwest while the negative stress coulomb leads to the southeast and northwest. This is due to the type of fault that is reverse fault. The earthquake, which is the result of a Monte Carlo simulation, was analyzed again with coulomb stress along with earthquakes that occurred from 2001 to 2021.

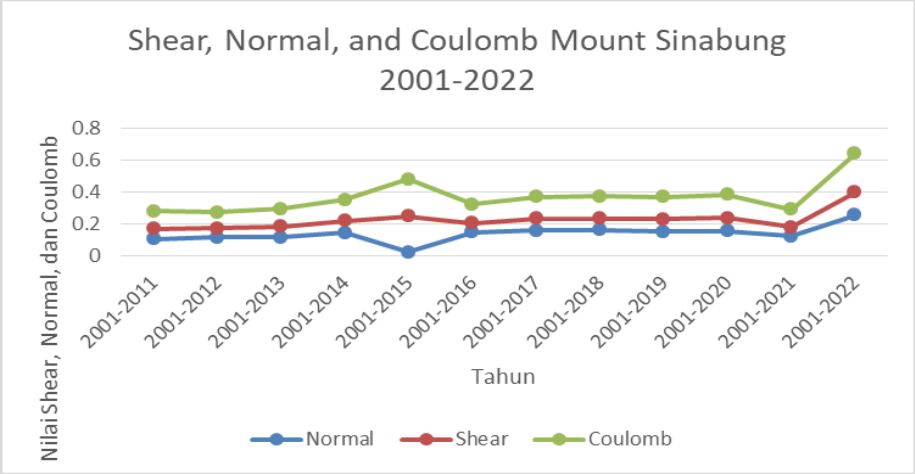

Figure 7 Graph of prediction of shear, Normal, and Coulomb values on Mount Sinabung 2001-2022

Based on the results of the coulomb stress change analysis from figure 7, obtained the average value of coloumb higher than 2021, namely coulomb value 0.24 bar, shear 0.14 bar, and normal 0.25 bar. The results of Coulomb 3.3 analysis also showed a greater direction of stress spread than in previous years.

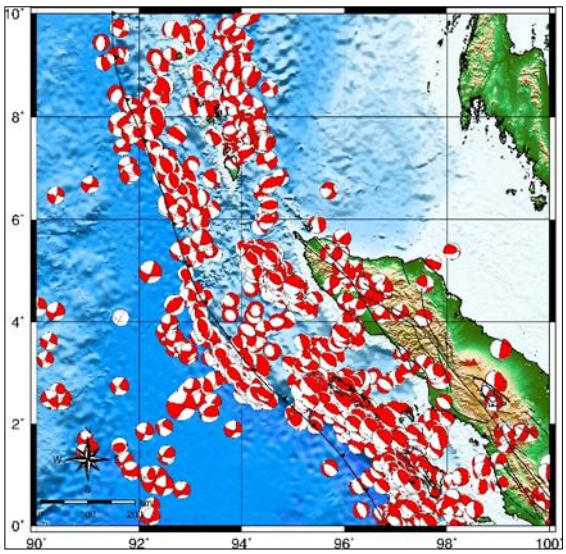

Figure 8 Map of earthquake distribution with Centroid Moment Tensor in 2022 (Monte Carlo Simulation Results)

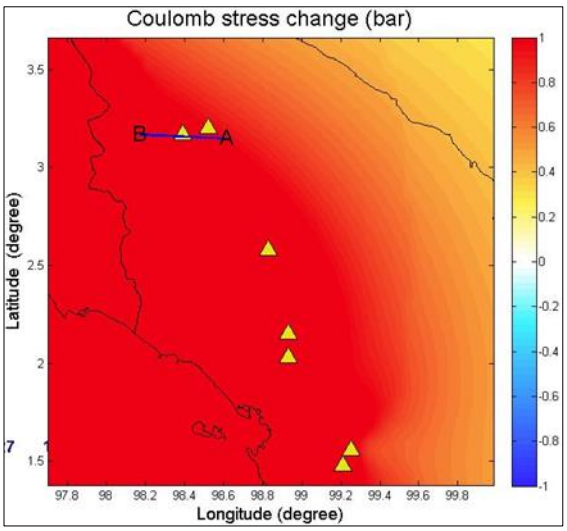

Figure 9 Prediction of Spread of Coulomb Stress Change in Mount Sinabung in 2022

Figure 8 shows a map of the distribution of earthquakes with centroid tensor moments from each event that occurred in 2021 and the 2022 earthquake (Monte Carlo simulation results). Centroid moment tensor that shows strike-slip fault, reverse fault, and normal fault. Centorid moment tensor is dominated by reverse fault, strike-slip fault, and normal fault. The distribution of earthquakes is influenced by regional geological conditions.

Figure 9 This is the result of Coulomb 3.3 analysis of prediction data that will occur in 2022 on Mount Sinabung. Mount Sinabung which experienced a spread of Positive Coulomb Stress Change in 2021 which is greater than in previous years. The increase in Coulomb value is due to the results of analysis of prediction data that is the result of Monte Carlo simulations that can be categorized as increasing positive coulomb stress changes around Mount Sinabung.

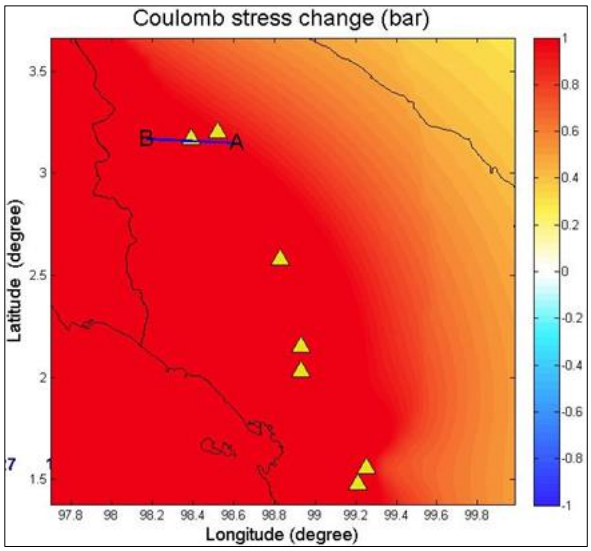

Figure 10 Prediction of Spread of Coulomb Stress Change on Mount Sinabung in depth of 0-100 km

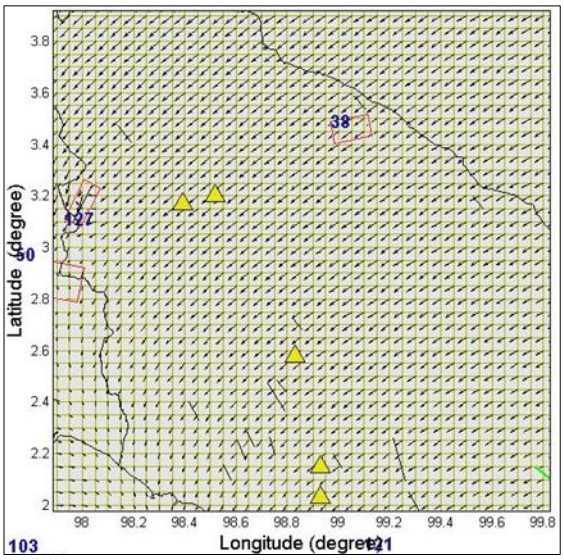

Figure 11 Horizontal Displacements vector Analysis Results

Figure 12 3D Vector Results

Figure 13 Sinabung Peak Condition

Figure 10 is the cross section of the distribution of coulomb stress changes under Mount Sinabung in 2022 at a depth of 0-100 km. In the image of cross section A-B in areas that experience increased stress is more inclined towards the northwest, west, southwest, south and southeast. If the Coulomb Stress analysis is converted in the direction of the stress vector then the direction of the positive coulomb spread of stress is dominant to the southwest as shown in figure 11.

Based on the results of horizontal displacement vector and 3D vector analysis in figure 12, the results of the positive Coulomb Stress spread are more inclined to the southeast. However, if you look at the gradient of the Coulomb vector line against the direction of pyroclastic flow, it can be assumed that pyroclastic flow is directly proportional to the direction of the Coulomb vector as far as 180^o. This hypothesis is based on Newton I's law which states that objects will move if the resultant forces working on the object equal to zero. (F=0).

$$\sum F = 0$$
$$F_{stress} + F_{fluida} = 0$$
$$F_{stress} = - F_{fluida}$$
$$\Delta CFF = -F_{fluida}$$
$$\Delta\tau + \mu\Delta\sigma = -F_{fluida}$$
$$F_{pyroclastic} = - (\Delta\tau + \mu\Delta\sigma)$$

F_{stress} can be assumed to be the stress caused by an earthquake accompanied by parameters of magnitude moment, depth, strike, slip, dip, and type of fault. While Ffluids can be assumed the thrust force of pyroclastic flow consists of characteristics (temperature, density, pressure, fluid density) and material composition (hydrogen, carbon monoxide,

carbon dioxide, hydrogen sulfide, sulfur dioxide, sulfur trioxide, chlorine and hydrochloric acid) pyroclastic. Theoretically, the direction of pyroclastic flow is inversely proportional to the direction of coulomb stress Change but pyroclastic flow can lead to the southeast or south. This is caused by the peak of mount Sinabung experiencing landslides in the east and southeast caused by eruptions that have occurred, so that the direction of pyroclastic flows changes to the east and southeast as in figure 13.

The results of the positive stress spread which is a combination of Monte Carlo simulation and coulomb stress analysis provide information that the data predicts the area of Mount Sinabung northeast, east, southeast, and south will become a pyroclastic watershed so it needs to get full attention and also become a warning area prone to volcanic disasters that are likely to erupt. The areas that must be given full warning and supervision are Bakerah Village, Sukameriah, Simacem, Sukanalu, Kutatonggal, Gamber, Gurukinayan, Berastepu, Sibintun, Mardinding, Perbaji, Kutagugung, and Sigarang-garang. The areas around Mount Sinabung especially in the north, east, and south have the potential to become pyroclastic watersheds (41).

4. Conclusion

The results of a combination of Coulomb Stress analysis and Monte Carlo Simulation of 2001-2021 earthquake data that occurred in northern Sumatra (wave magnitude, depth, coordinates, fault type) resulted in a greater prediction of the value and spread of positive Coulomb Stress changes in 2022 than in 2021. Monte Carlo simulations produced a longitude of 98^{o} latitude 3.175^{o} depth 104.5 meters, Mw 6.0, strike 28.125^{o}, slip 42^{o}, dip 44.17^{o}. While the Coulomb Stress analysis of the combined earthquake data 2001-2021 resulted in an average value of Coulomb 0.24 bar, shear 0.14 bar, and normal 0.25 bar. Coulomb stress analysis also provides a stress vector direction to the southwest of Mount Sinabung. The results of a combination of coulomb stress analysis and Monte Carlo simulations predict the direction of pyroclastic flows to the northeast, east, and southeast in accordance with the direction inversely proportional to positive stress so that the area needs to get an early warning of natural disasters in 2022.

Compliance with ethical standards

Acknowledgments

The author thanked several parties namely BMKG Indonesia, PVMBG Indonesia, USGS, and Global CMT for their contributions in providing earthquake data and volcanic activity that can be accessed. Hopefully the results of this study can provide benefits to all parties for natural disaster mitigation.

Disclosure of conflict of interest

The author and other members of the author have contributed to the implementation of research both in surveys, data collection, data analysis, and reporting in paper form so that research results can be realized in the form of research papers.

References

[1] H Gunawan et al. Overview of the eruptions of Sinabung Volcano, 2010 and 2013–present and details of the 2013 phreatomagmatic phase, J. Volcanol. Geotherm. Res. 2019; 382: 103–119.

[2] E Chaussard, F Amelung. Precursory inflation of shallow magma reservoirs at west Sunda volcanoes detected by InSAR, Geophys. Res. Lett. 2012; 39(21): 6–11.

[3] CW Lee, Z Lu, JW Kim, SK Lee. Volcanic activity analysis of Mt. sinabung in Indonesia using InSAR and GIS techniques, Int. Geosci. Remote Sens. Symp. 2015; 1: 4793–4796.

[4] M Iguchi, K Ishihara, Surono, M Hendrasto. Learn from 2010 Eruptions at Merapi and Sinabung Volcanoes in Indonesia Masato IGUCHI, Kazuhiro ISHIHARA, SURONO *,Disaster Prev. Inst., Kyoto univ. 2011; 54.

[5] M Hendrasto, et al. Evaluation of volcanic activity at sinabung volcano, after more than 400 years of quiet, J. Disaster Res. 2012; 7(1): 37–47.

[6] S Andreastuti, ET Paripurno, H Gunawan, A Budianto, D Syahbana, J Pallister. Character of community response to volcanic crises at Sinabung and Kelud volcanoes, J. Volcanol. Geotherm. Res. 2019; 382: 298–310.

[7] J Pallister, et al. Monitoring, forecasting collapse events, and mapping pyroclastic deposits at Sinabung volcano with satellite imagery, J. Volcanol. Geotherm. Res. 2019; 382: 149–163.

[8] ML Bell, A Nur. Strength Changes Due To Reservoir-Induced Pore Pressure and Stresses and Application To Lake Oroville.," J Geophys Res. 1978; 83(B9): 4469–4483.

[9] M Parotidis, E Rothert, SA Shapiro. Pore-pressure diffusion: A possible triggering mechanism for the earthquake swarms 2000 in Vogtland/NW-Bohemia, central Europe," Geophys. Res. Lett. 2003; 30(20): 10–13.

[10] SA Shapiro, R Patzig, E Rothert, J Rindschwentner. Triggering of seismicity by pore-pressure perturbations: Permeability-related signatures of the phenomenon, Pure Appl. Geophys. 2003; 160(5–6): 1051–1066.

[11] S Talwani, P Acree. Pore pressure diffusion and the mechanism of reservoir-induced seismicity, Pure Appl. Geophys. 1984; 122(6): 94.

[12] MD Zoback, SM Gorelick. Earthquake triggering and large-scale geologic storage of carbon dioxide, Proc. Natl. Acad. Sci. U. S. A. 2012; 109(26):10164–10168.

[13] SPAG (GAW), B Kototabang, BMK dan Geofisika. HUBUNGAN ANTARA GEMPABUMI DENGAN ERUPSI GUNUNGAPI STUDI KASUS ERUPSI GUNUNG SINABUNG TAHUN 2010 DAN 2013, Megasains. 2013; 4: 117– 123.

[14] P Monte, C Untuk. Pemodelan monte carlo untuk prediksi sifat hujan harian 1,2,3. 2020; 2: 124–135.

[15] Shinji Toda, Ross S. Stein, Volkan Sevilgen and Jian Lin. Coulomb 3.3 Graphic-Rich Deformation and Stress-Change Software for Earthquake, Tectonic, and Volcano Research and Teaching— User Guide. Virginia: U.S. Geological Survey, Reston, Virginia. 2011.

[16] GCP King, RS Stein, Jian Lin. Static stress changes and the triggering of earthquakes, Bull. - Seismol. Soc. Am. 1994; 84(3): 935–953.

[17] W Simpson. Response of Regional Seismicity. 1992; 6: 1687–1690.

[18] RA Harris. Introduction to special section: Stress triggers, stress shadows, and implications for seismic hazard, J. Geophys. Res. Solid Earth. 1998; 103(10): 24347–24358.

[19] KM Keranen, HM Savage, GA Abers, ES Cochran. Potentially induced earthquakes in Oklahoma, USA: Links between wastewater injection and the 2011 Mw 5.7 earthquake sequence, Geology. 2013; 41(6): 699–702.

[20] JR Rice, MP Cleary. Some basic stress diffusion solutions for fluid-saturated elastic porous media with compressible constituents, Rev. Geophys. 1976; 14(2): 227–241.

[21] DH Green, HF Wang. "ap,". 1986; 51(4): 948–956.

[22] DJ Hart, HF Wang. limestone of the pore E = all K •,., J. Geophys. Res. Solid Earth. 1995; 100(95): 741–751.

[23] M Cocco. Pore pressure and poroelasticity effects in Coulomb stress analysis of earthquake interactions, J. Geophys. Res. 2002; 107(B2).

[24] JR Rice. Fault Stress States, Pore Pressure Distributions, and the Weakness of the San Andreas Fault, Int. Geophys. 1992; 51(C): 475–503.

[25] T Parsons, RS Stein, RW Simpson, PA Reasenberg. Stress sensitivity of fault seismicity: A comparison between limited-offset oblique and major strike-slip faults, J. Geophys. Res. Solid Earth. 1999; 104(B9): 20183–20202.

[26] RS Stein, GCP King, J Lin. Change in failure stress on the San Andreas and surrounding faults caused by the 1992 M=7.4 Landers earthquake, Science (80-.). 1992; 258: 1328–1332.

[27] S Toda, J Lin, RS Stein. "Using the 2011 Mw 9.0 off the Pacific coast of Tohoku Earthquake to test the Coulomb stress triggering hypothesis and to calculate faults brought closer to failure, Earth, Planets Sp. 2011; 63(7): 725–730.

[28] T Yamasaki, TJ Wright, G Houseman. Journal of Geophysical Research : Solid Earth, AGU J. Geophys. Res. Solid Earth. 2014; 119: 3678–3699.

[29] KJ Wells, Donald L. Coppersmith, No New empirical relationships among magnitude, rupture length, rupture width, rupture area, and surface displacement. United States: Seismological Society of America, Berkeley, CA, United States. 1994.

[30] B Satya. Simulasi, Teori dan Aplikasinya. Yogyakarta. Indonesia: Penerbit Andi. 2007.

[31] N Indrastuti, et al. 3-D Seismic Tomographic study of Sinabung Volcano, Northern Sumatra, Indonesia, during the inter-eruptive period October 2010–July 2013, J. Volcanol. Geotherm. Res. 2019; 382: 197–209.

[32] M Madlazim. Coulomb Stress Changes Due To Recent Aceh Earthquakes, J. Penelit. Fis. dan Apl. 2015; 5(1): 9-14.

[33] P Coulomb, S Gempabumi, SM September. Coulomb Stress Change of Mw 7 . 5 Palu-Donggala Earthquake, Sulawesi. 2018; 18(01): 19–22.

[34] MI Titi Andriani, Muhammad Hidayatullah. Jurnal Ilmu Fisika. 2018; 10(2): 103–112.

[35] GHD Sinaga, M Zarlis, M Sitepu, RA Prasetyo, A Simanullang. Coulomb stress analysis of West Halmahera earthquake mw=7.2 to mount Soputan and Gamalama volcanic activities, IOP Conf. Ser. Earth Environ. Sci. 2017; 56(1): 3–10.

[36] FA Pratikno, G Rachman, BJ Santosa. Coulomb Stress Analysis of Halmahera. 2019; 30(2): 41–44.

[37] S Nakada, et al. Eruption scenarios of active volcanoes in Indonesia, J. Disaster Res. 2019; 14(1): 40–50.

[38] M Utkucu, H Durmuş, H Yalçın, E Budakoğlu, E Işık. Coulomb static stress changes before and after the 23 October 2011 Van, eastern Turkey, earthquake (<i>M</i>_W= 7.1): implications for the earthquake hazard mitigation," Nat. Hazards Earth Syst. Sci. 2013; 13(7): 1889–1902.

[39] Z Zhou, TM Kusky, CC Tang. Coulomb stress change pattern and aftershock distributions associated with a blind low-angle megathrust fault, Nepalese Himalaya, Tectonophysics. 2019; 767: 228161.

[40] B Maleki Asayesh, S Zarei, H Zafarani. Effects of imparted Coulomb stress changes in the seismicity and cluster of the December 2017 Hojedk (SE Iran) triplet, Int. J. Earth Sci. 2020; 109(7): 2307–2323.

[41] A Loeqman. Pemodelan Aliran Awanpanas (Aliran Piroklastik) Sebagai Data Pendukung Peta Kawasan Rawan Bencana Gunungapi (Studi Kasus Gunungapi Sinabung Sumatra Utara), J. Lingkung. dan Bencana Geol. 2017; 8(1): 1.